Journal Name

ARTICLE

Cavitation clusters in lipid systems – surface effects, local heating and streamer formation

P. R. Birkin,[a†] T. M. Foley,[a] T. T. Truscott[b], A. Merritt[c] and S. Martini[c]

aReceived 00th January 20xx,
Accepted 00th January 20xx

DOI: 10.1039/x0xx00000x

www.rsc.org/

Cavitation clusters and streamers are characterised in lipid materials (specifically sunflower oil) and compared to water systems. The lipid systems, which are important in food processing, are studied with high-speed camera imaging, laser scattering and pressure measurements. In these oils, clusters formed at an aged (roughened) tip of the sound source (a piston like emitter, PLE) are shown to collapse with varied periodicity in relation to the drive amplitude employed. A distinct streamer (an area of increased flow emanating from the cavitation cluster) is seen in the lipid media which is collimated directly away from the tip of the PLE source whereas in water the cavitation plume is visually less distinct. The velocity of bubbles in the lipid streamer near the cluster on the order of 10 m s^{-1}. Local heating effects, within the streamer, are detected using a dual thermocouple measurement at extended distances. Viscosity, temperature and the outgassing within the oils are suggested to play a key role in the streamer formation in these systems.

Introduction

Lipids are used extensively in the food industry and play a key role in the structure and palatability of a variety of food materials. Lipids are added as they have unique physical properties, which enhance the quality of foods. Important physical properties of edible lipids include crystal size, melting behaviour, polymorphism, and viscoelasticity. Accurate control of lipid crystallization is desirable for these qualities to be obtained[1]. Hence a variety of processing technologies have been developed to control and produce a number of different material characteristics. Amongst these technologies is the application of acoustic energy[1–8]. In particular, the use of high intensity ultrasound (HIU) has been used to alter the properties of lipids[5]. HIU can be used to induce the crystallization of edible lipids such as shortenings and generate crystalline materials that are harder, more viscous, more elastic, and that have smaller crystals that melt over a narrower temperature range compared to their non-sonicated counterparts. The impact and significance of using this technology is that it can be used in lipids with low content of saturation. In 2015 the Food and Drug Administration (FDA) has eliminated the Generally Recognized as Safe (GRAS) status of partially hydrogenated oils due to their detrimental effect on human health. This new regulation has challenged food scientists to find alternative fat sources and processing technologies that can replace these hard fats in food formulations. HIU seems to be a promising processing alternative to generate these harder materials in healthier fats that are free of *trans*-fats and that have lower content of saturated fatty acids. Previous research has shown that HIU was effective in several edible lipids including anhydrous milk fat[9], all-purpose shortening[1], interesterified soybean oil[5,7], palm oil[2,6], and coconut oil[10] among others. Although HIU has a significant effect on the crystallization dynamics of all these lipids, sonication conditions must be optimized for each lipid type. The underlying physical mechanisms that play a role in these lipid systems remain unknown. It is likely that cavitation dynamics and the resultant bubble population play a key role in the process. In addition, shear forces (on the liquid and the solid materials within the liquid) and the energy input influence these processes. Experiments performed in water provide a useful first approximation. For example, the piston like emitter (PLE) is a common sound source employed in HIU applications. The PLE system has been shown to produce a complex environment where hot spots[11,12], bubbles, bubble clusters[13–15], inertial[16,17] cavitation and non-inertial[18–20] cavitation exist and where different processes may be driven (for example surface erosion[21,22], chemical changes[23–27] and mass transfer[28–30] effects). While many experimental studies of these effects in water environments exist, oils, and in particular lipids[31] have received little fundamental investigation. Hence, it is timely, particularly considering the technological significance of this material, to characterise and contrast the cavitation fields that are generated in these liquid materials as reported here. The objective of this research is therefore to analyse the formation of cavitation clusters in a liquid oil and characterize changes observed in the system due to sonication. A vegetable oil, such as sunflower oil will be used as a model system to study bubble dynamics in the absence of crystals (note that if a commercial shortening is used, crystallization occurs immediately after

[a] *Chemistry, University of Southampton, Southampton, UK, S017 1BJ.*
[b] *Department of Mechanical and Aerospace Engineering, Utah State University, Logan, UT, 84322-4130, USA.*
[c] *Department of Nutrition, Dietetics, and Food Science, Utah State University, Logan, UT, 84322-8700, USA.*
† author for correspondence, prb2@soton.ac.uk.
Electronic Supplementary Information (ESI) available: [details of any supplementary information available should be included here]. See DOI: 10.1039/x0xx00000x

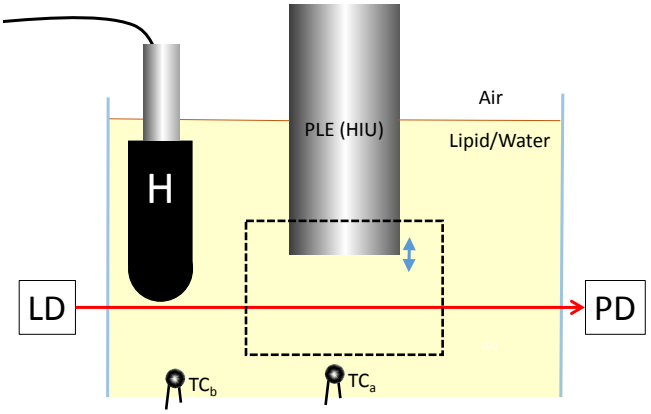

Figure 1. Schematic representation of the experimental setup employed for the laser scattering, acoustic, temperature and high-speed imaging experiments. Note the active centre of the hydrophone was placed at the same height as the PLE tip and with a lateral distance of ~ 1-2 cm. The dotted square represents the area imaged with the high-speed camera (4.65 mm x 4.65 mm). LD represents the laser diode, PD the photodiode, TC_a and TC_b are the thermocouples and H the hydrophone. Not to scale.

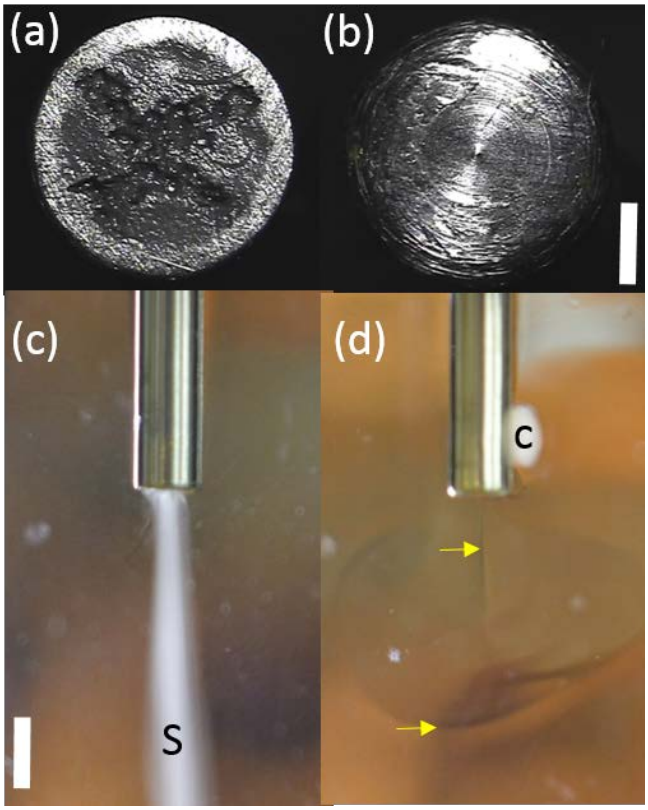

Figure 2. Images taken to demonstrate tip surface effects. (a) eroded tip, (b) fresh tip, (c) side view of cluster and streamer activity on tip (a). (d) shows a side view of a cell with tip (b). In (c) 'S' represents the stable streamer formed under these conditions. In (d) there is an unstable cluster annotated 'C' and clear refractive index changes highlighted with yellow arrows. The scale bar represents 1 mm for (a) and (b) and 3.2 mm for (c) and (d). The cell contained aerobic sunflower oil at ~20°C. The probe was driven at ~5 W_{rms} in both cases.

sonication and the subsequent crystals would interfere with the observation of relevant bubble dynamics).

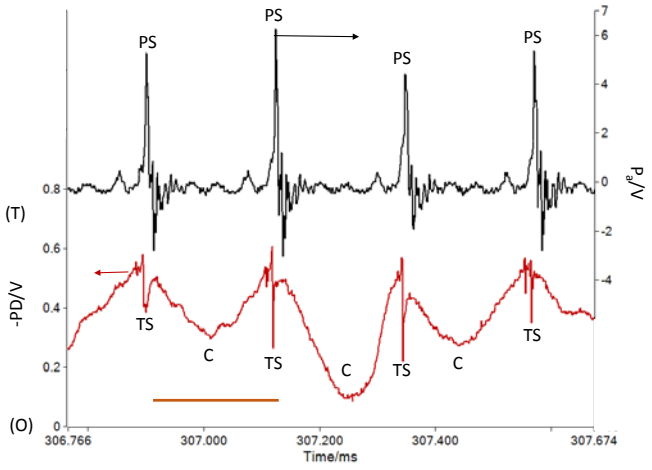

Figure 3. Plots showing the acoustic emission detected by the hydrophone (— P_a) and the photodiode signal (— PD, note the axis is inverted for clarity) recorded simultaneously in a lipid system (aerobic sunflower oil). The 3.2 mm diameter tip was driven at 33 W_{rms} at ~22.68 kHz. The lipid had an initial temperature of 18.9 °C. The path of the laser was positioned 2.5 mm below the tip. (T) and (O) represent the laser signal under transparent and opaque conditions respectively. TS, C and PS represent the transient signal due to bubble dynamics associated with pressure pulses in the system, the cluster and the pressure signal respectively. The scale bar represents 5 periods of the ultrasonic source.

Experimental

Cavitation was generated using a piston like emitter (Misonix) immersed in the liquid. The diameter of the titanium tip was 3.2 mm (P1 tip). Calorific characterisation of the output of the system (in the absence of a suitably calibrated pressure sensor) is reported in the SI data. High-speed imaging (using a Photron APX-RS camera and Navitar x12 or Sirius lens (70-210 mm) or a Phantom V2011 and a Sigma (105 mm) fixed lens with 50 mm extension tubes) of the tip within the oil system (sunflower, e.g. Independent) was also deployed. A calibrated hydrophone (Reson TC4013) was positioned ~ 2 cm to the side of the tip of the probe (itself 15 mm immersed into the oil). Note that the calibration of the hydrophone is assumed to have an inherent error within the oil system, however, for reference the sensitivity[32] is -2.66 x 10^{-5} V Pa^{-1} under these conditions at ~22.7 kHz in water. Figure 1 shows a schematic representation of the experimental arrangement employed for the high-speed imaging, acoustic measurements and light scattering experiments. Note a 60 mm x 60 mm x 150 mm polycarbonate cell was used to contain the lipid material (here sunflower oil). A digital oscilloscope (Owon DS7102V DSO) was used to capture the acoustic and light scattering data (sample rate 1 MHz). Temperature measurements were performed with K-type thermocouples (TM Electronics) and a datalogger (Picoscope, TC-08) interface. Velocity measurements at extended distances from the PLE tip (~ 2 cm) were enabled through bubble (particle) tracking of high-speed images. Stills images were captured using a Nikon D5200 with an 18-55 mm lens (see figure 2 (c) & (d)) or a JAI camera fitted with a Navitar x12 system(see figure 2 (a) & (b)).

Results and discussion

Figure 2 shows a collection of images designed to show how the condition of the tip of the PLE affects the dynamics of the cavitation environment within sunflower oil. If the tip is eroded (through use, see figure 2 (a)) a well-defined and stable cavitation plume was observed in sunflower oil (see figure 2 (c)). However, if a fresh (or polished) tip was used in the same media, the cavitation plume was ill defined, unstable and audibly different (see figure 2 (d)). These results are in contrast to those found in water where the cavitation plume was identical (from optical and acoustic observations, see SI information). These results imply that the tip condition is particularly important in defining the cavitation environment in the oil (lipid) matrix. Presumably, the rough surface acts as an excellent nucleation site that is necessary for the oil system to maintain reproducibility of the cluster formed at the tip of the PLE. However, this nucleation site is less important for water. This is likely to be associated with the intrinsic properties of the liquids themselves (such as viscosity and gas content, etc., see SI data). Several points are relevant here. First, the viscosity of the oil system is significantly higher than water[33]. This will affect the bubble dynamics, the inertial threshold[16] and the acoustic absorption[33] in the media. Second, the experiments were performed under 'steady state' conditions after the PLE tip has 'rung up' (see SI data for examples). In these cases, the oil can be considered to be populated with existing gas bubbles (as confirmed by visual and imaging observations). However, initiation of the cluster at the eroded tip occurs relatively rapidly (<200 ms) under these conditions even for an oil left undisturbed for 24 hours. The images recorded and shown in figure 2 for the eroded tip also show a cluster/collection of bubbles formed at the surface of the piston. These collections or clusters[13,14] of bubbles have been studied in a variety of experimental scenarios[34–36] and liquid matrices. However, it appears for the lipid material (e.g. sunflower oil) relatively little investigation of the dynamics in these systems have been reported. Further experiments were performed for the eroded tip as this was found to produce the most reproducible results in the oil system. Figure 3 shows a collection of the results gathered from the laser scattering and acoustic measurements performed in the oil system. For example, the hydrophone data (—) shows the signal from the sound source (22.68 kHz) and a regular set of high pressure pulses or shocks (labelled PS). The output from the photodiode (—) shows that the liquid ~2.5 mm below the PLE becomes periodically semi- transparent in the path of the laser through the lipid media (note this distance was chosen as it is relatively close to the PLE tip/cluster but not so close as to be completely occluded by the tip/cluster at any time). This dynamic opacity is linked to the periodicity of the hydrophone signal. Here the liquid becomes more transparent (note a more negative voltage) before the pressure pulse (PS) is observed in the hydrophone data (see figure 3 for example). At the moment of maximum transmission of the laser through the oil, a set of transient events are also detected in the laser scattering data. This has been observed before in water based systems[37] and corresponds to the response of the bubble population to the PS event. Briefly, bubbles within the media are compressed and rebound (resulting in transient changes in laser transmission through the oil, in this case). These events are labelled TS and occur at regular intervals within the data set shown and precede the pressure pulse as a result of a time of flight delay of the acoustic signal with respect to that for the laser signal. The events that cause the pressure signal and changes in the light transmission through this zone are linked to cluster dynamics and the subsequent dynamic response of the bubble population within the liquid. Note also that under the conditions deployed the cluster dynamic was observed (with a high-speed camera) to have a periodicity of $f/5$, where f represents the period of the ultrasonic source employed (specifically the PLE at 22.68 kHz). Further observations are noteworthy; the audible noise emitted by the system was observed to vary significantly with the drive amplitude of the PLE. Figure 4 shows a collection of the frequency components present in the hydrophone data following appropriate FFT analysis (note the amplitudes of each frequency component are kept in volts here as the sensitivity of the hydrophone in oil is unknown at this time) of the hydrophone signal. In each case the data for each of the traces corresponds to a different audible 'note' determinable by ear.

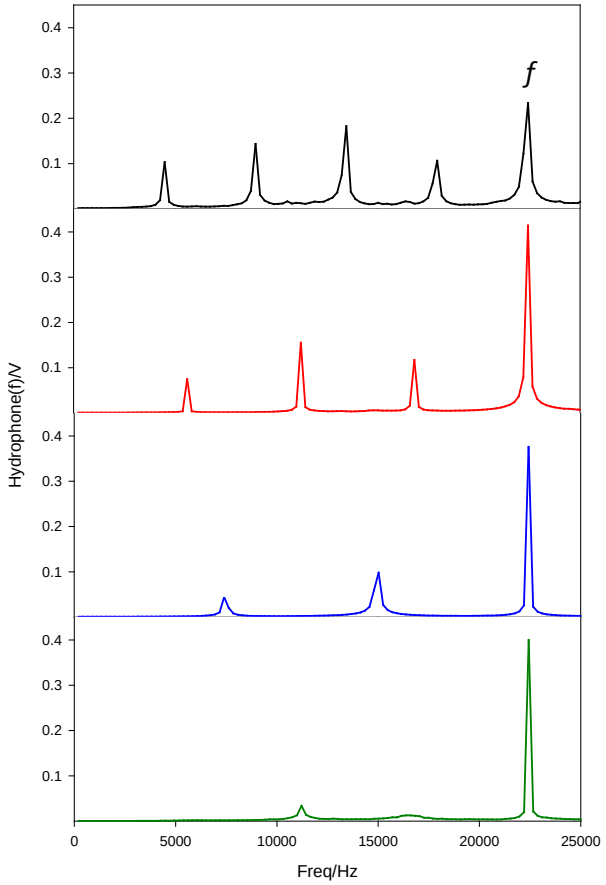

Figure 4. Plots showing the frequency analysis of the hydrophone data recorded under different drive conditions. The power settings for the PLE were 43 (—), 24 (—), 13 (—) and 8 (—) W_{rms}. The liquid was aerobic sunflower oil at ~20°C. Note f here is the PLE fundamental frequency (22.68 kHz).

Figure 4 shows that a distinct set of subharmonics are present with the number of subharmonic components increasing as the drive amplitude of the PLE was increased (note here the rms output of the amplifier is noted for reference, see SI for further calibration data). Each distinct 'note' and its resultant frequency components, are annotated with a *f*/*N* nomenclature. Here *f* refers to the drive frequency of the PLE while *N* is an integer value (here 2-5). In each case a set of subharmonics are detected in a sequence comprising of *nf*/*N* where *n* = 1 to *N*-1 in integer steps. For simplicity we refer to each case with the *f*/*N* nomenclature. It is also interesting to comment on the use of the *f*/2 subharmonic to monitor cavitation activity in this system. Clearly figure 4 shows that the *f*/2 component is only present for the even clusters (e.g. *f*/2 and *f*/4 for the range of experiments shown). This implies that a more sophisticated analysis of the subharmonic[38] frequency band would be appropriate for these stable cluster systems. The origin of these subharmonic frequency components is likely to be associated with the cluster dynamics at the tip of the PLE. In order to validate this assumption a set of complimentary experiments were undertaken. In this case, high-speed imaging and acoustic measurements were employed simultaneously to characterise the dynamics of the cluster (or cavitation events) at the surface of the PLE.

Figure 5 shows the dynamics of the cavitation cluster that was generated at the tip of the PLE employed under different drive conditions. Figure 5 (a) shows clear evidence for a cluster that repeats every 12 frames (~171 µs corresponding to ~4 periods of the PLE) while figure 5(b) shows a set of images for a cluster repeating every 16 frames (~229 µs corresponding to ~5 periods of the PLE). These cluster events have acoustic emission data that possess subharmonics at *f*/4 and *f*/5 for figure 5 (a) and (b) respectively. This suggests that the periodicity of the subharmonic emission is strongly linked to the cluster periodicity itself as expected. While this data is useful, further experiments were performed to gather information on the final stage of collapse and to observe in more detail the dynamics that occur within the environment close to the PLE/cluster. Figure 6 shows an *f*/5 cluster at the point of collapse. These images are in agreement with figure 5 and show that the shape of cluster formed at the tip of the PLE appears to have three distinct sections. The 'arrowhead' (region (iii)) appears to detach from the main cluster forming a longer 'neck' (region (ii)) and a 'ring' (region (i)) are marked on figure 6. Figure 6 shows that the collapse phase of the cluster is relatively rapid (on the 10 µs time window available from this data, see figure 6 ●, ●) before the cluster starts to reform (see figure 6 bottom row of images). Figure 7 shows the region just below the cluster prior to collapse (a), at cluster collapse (b) and just after cluster collapse (c). Figure 7(a) indicates that the gas bubbles in this environment appear elongated, are compressed (b) and then rebound (c). This agrees with the scattering data (see figure 3) which indicated a momentary increase in light transmission followed by a rebound ('transient flash', which cause temporary drops in light transmission) which are associated with the pressure shock generation observed in this and water systems. However, the images shown in figure 7 also indicate that the

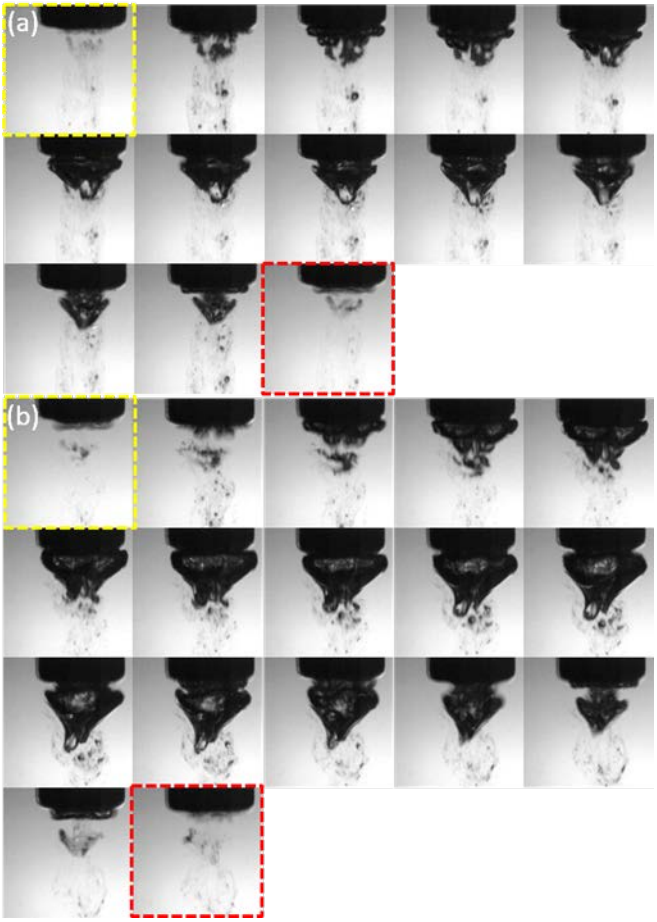

Figure 5. Collections of images from high-speed camera characterisation of the stable clusters and formed on an aged tip in sunflower oil. Panel (a) shows the cluster dynamics and periodicity recorded (70 kfps, shutter speed 14.3 µs) shows a cluster periodicity corresponding to *f*/4 (shown as the time interval between yellow and red highlighted frames) as determined by acoustic emission analysis. Panel (b) shows the cluster dynamics and periodicity recorded corresponding to *f*/5 (shown as the time interval between yellow and red highlighted frames) as determined by acoustic emission analysis. The PLE was 3.2 mm in diameter and each frame was ~4.6 mm x 4.6 mm square. Note the sequences should be read from top left to right in a raster fashion.

environment is more complex with non-spherical bubbles (including trains or elongated bubbles, see figure 7 (a) red arrows) appearing within the fluid. The high-speed images also show that a stream of bubbles is emitted from the base of the cluster. This streamer was observed to extend for a particularly long distance (to the base of the cell ~ 10 cm in length). In addition, it is relatively compact and particle tracking close to the cluster (within 10 mm) show that the velocity within this restricted zone was on the order of 10 m s^{-1} (see SI, figure S2). However, fluid flow in the streamer further from the tip (~2 cm) yields flow rates in the range 1-2 m s^{-1} indicating that the flow is position dependant as one would expect in a viscous jet flow field, considering the shape of the sound field and losses due to viscosity of the media. Nevertheless, these velocities are not insignificant. For example, comparative measurements in water[39] indicate an average velocity of 2.450 ± 0.370 m s^{-1} at ~5 mm from the PLE.

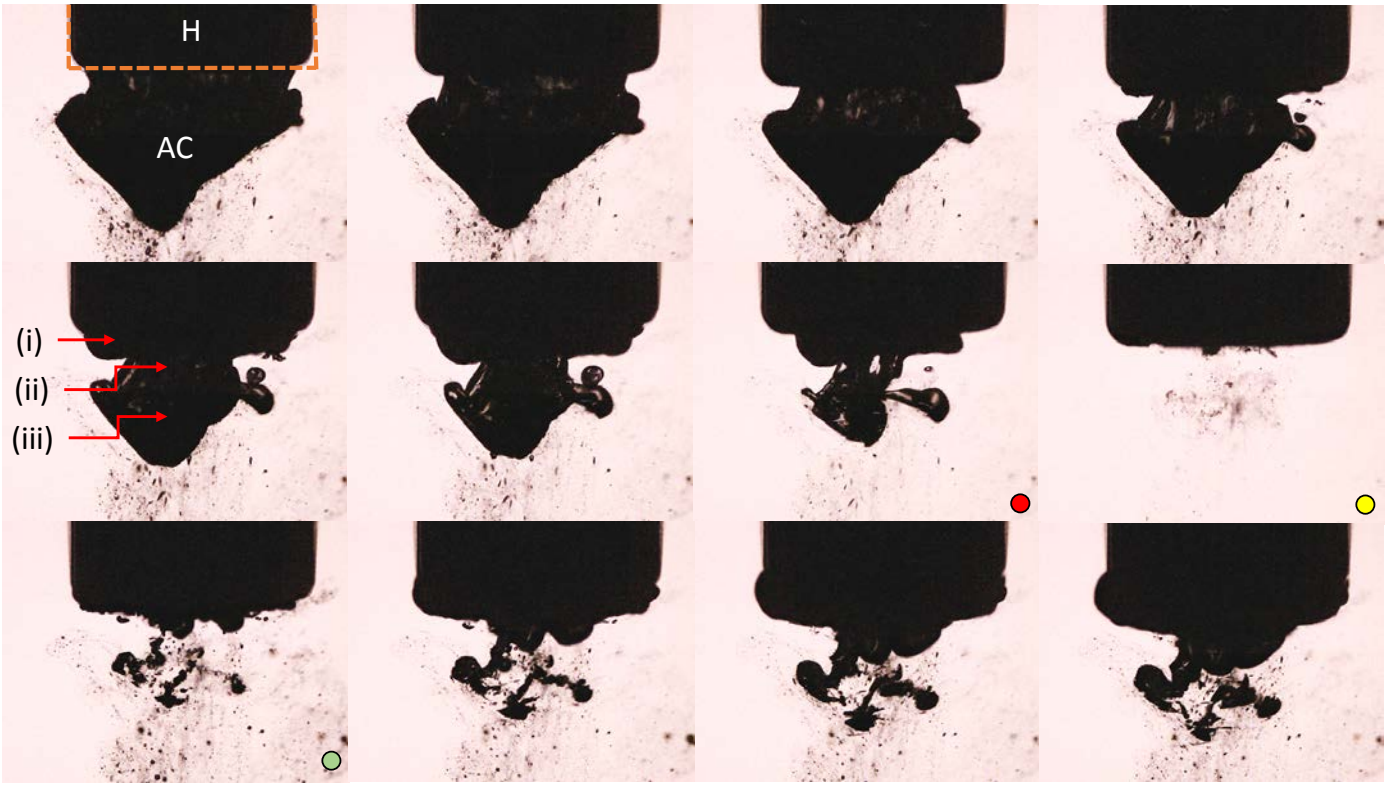

Figure 6. High resolution, high-speed images of the final moments of a single *f*/5 cluster during the collapse phase. The annotation '(i)', '(ii)' and '(iii)' show the 'ring', 'neck' and 'arrowhead' structure that form repetitively during the lipid cluster events. The images were recorded at 99.8 kfps with a 0.9 µs shutter speed. The first frame shows the outline of the PLE (H) and the cluster (AC). Each frame shows an region of the fluid which is 3.38 x 4.51 mm in size. The frames marked with ●, ●, ● are discussed in figure 7. Note the sequences should be read from top left to right in a raster fashion.

The imaging of the cluster and streamer also shows some evidence for refractive index changes, observed as what can be described as a 'shimmer'. The extent of this temperature differential between the bulk and the fluid moving in the streamer can be estimated by measuring the local temperature in the oil within the streamer and in the bulk.

Figure 8 shows the results from a set of experiments employing two thermocouples (TC_a in the streamer, TC_b within the bulk, see figure 1). Figure 8(a, b) shows the positioning of the thermocouples with respect to the PLE. The thermocouples were positioned so that they could detect the temperature in the streamer (or bulk) but to avoid perturbing the cluster. Figure 8 (c) shows the temperature time profiles recorded from the two thermocouples as the PLE was energised for a sequence of 10 s bursts. The temperature profiles recorded were dependant on the power supplied to the PLE. For example, at 16 W_{rms} an *f*/4 cluster was generated (determined by characterising the acoustic emission). Here the streamer is ~ 1 ^{0}C higher in temperature compared to the bulk and which shows evidence for flow induced cooling (presumably due to cooler fluid near the edge of the cell being drawn over TC_b). However, if the drive amplitude was increased to 25 W_{rms} (note an *f*/5 cluster) the temperature differential is still apparent while the presumably more rapid motion of the liquid results in greater homogeneity between the two thermocouple measurements. It is possible to estimate whether these temperature variations are reasonable. Consider the case where a 1 m s^{-1} flow within the streamer (~ 1.5 mm in radius) impinges on TC_a. Under these conditions an estimated heating input to the oil can be calculated as ~ 13 W. This is reasonable compared to the energy inputs deployed in this study (up to 25 W_{rms} in figure 8) particularly considering the uncertainties in the streamer dimensions, velocities encountered, and other energy losses which are unaccounted for in this calculation.

Further complimentary temperature measurements and characterisation techniques (e.g. Schlieren imaging[40–43]) of these systems would be valuable but are beyond the scope of this investigation. Finally, the data presented thus far indicates that the cluster dynamics and streamer formation characteristics in oil are similar to those seen in water but with a number of interesting caveats (for example, local fluid heating and the narrow nature of the extended streamer observed). One major difference between the two systems (water and lipid/oil) is that the viscosity of the lipid system is significantly raised when compared to water. For example, lipids typically have viscosities of the order of 84 cP compared to water which has a viscosity of 1.0019 cP at the same temperature[33]. In addition, the gas content of the oil is reported to be significantly greater than water. Battino *et al.* reported that the mole fraction of nitrogen in olive oil is 2.82 x 10^{-3} whereas in water it is reported as 1.18 x 10^{-5} under the same conditions[44]. The significant differences in gas solubility and viscosity as well as

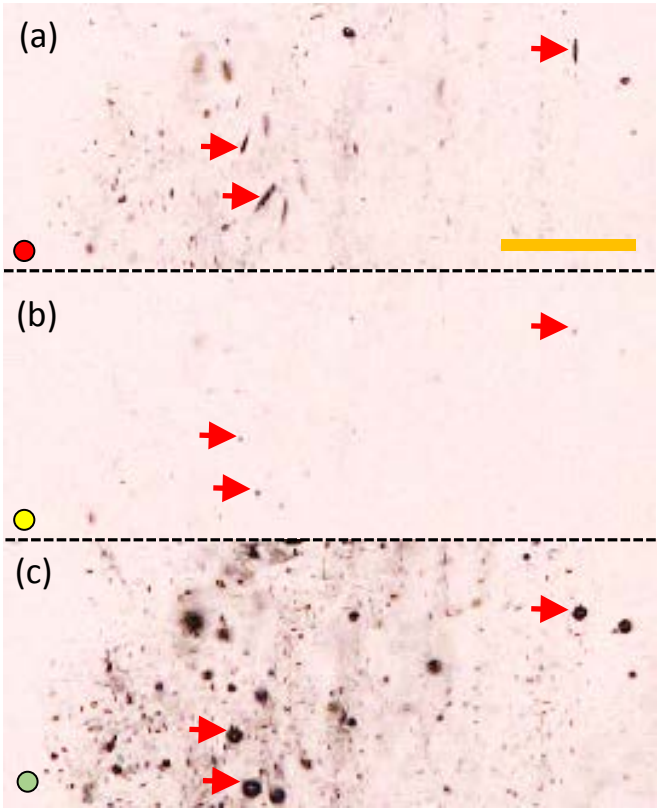

Figure 7. Images showing an enlargement of the region just below the cluster just prior to, (a), at cluster collapse, (b) and after collapse (c) taken from the images shown in figure 6 (marked with ●, ●, ●). Note the arrows indicate gas bubbles (or trains of bubbles) within the liquid. The images show how these bubbles are compressed (and hence almost disappear from view) and then rebound during this sequence. The scale bar (a) represents 500 µm.

the local heating generated (see figure 8 and SI data, which will also change the local viscosity of the system) help to explain some of the differences seen in these lipid systems when compared to aqueous solutions. The streamer that forms in this system does not seem to have any banding which indicates that primary Bjerkness forces do not seem to play a major role under the conditions stated (see SI for further discussion). However, the effects of bubble/bubble interactions[45] require further investigation. Lastly, the formation of bubbles near the PLE tip (that propagate downstream) may also have consequences for the optical clarity of the lipid/oil system. However, while this effect may be significant for nucleation processes in the treatment of food stuffs, further complimentary experiments are needed to ascertain the relative contributions of the gas content/viscosity variations that may be affected by local heating effects detected herein.

Conclusions

The generation of cavitation in the oil/lipid system shows some remarkable characteristics. For an aged PLE tip, the acoustic, high-speed imaging and scattering data show that the sound source amplitude plays a key role in the dynamics of the cavitation cloud. The cavitation cloud in the oil systems forms a set of well-defined clusters/large gas bubbles which collapse under the conditions employed at a variety of different periods (ranging from *f*/2-*f*/5 under the conditions reported here) relating to the amplitude of the drive applied to the PLE. The streamer that forms in these systems is dynamic with velocities on the order of 10 m s^{-1} close to the tip of the PLE while remaining ~2 m s^{-1} at extended distances from the tip of the

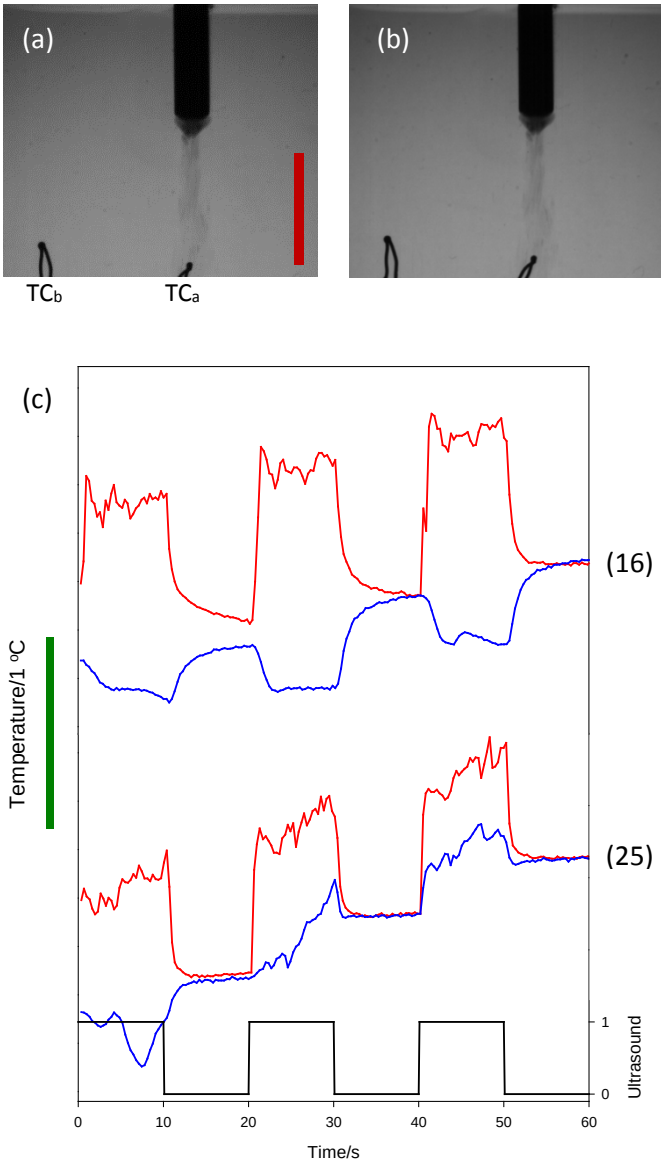

Figure 8 (a) Image of streamer (25 W_{rms}, *f*/5 periodicity) forming in the cell and flowing over TC_a. TC_b is shown outside the streamer on the left. The scale bar represents 1 cm. (b) Image of streamer (16 W_{rms}, *f*/4 periodicity) forming in the cell and flowing over TC_a. TC_b is shown outside the streamer on the left. For scale purposes, the PLE (upper centre) is 3.2 mm in diameter. (c) Temperature time profiles for 10 s on/off exposure of the sample by 22.68 kHz ultrasound. The power input to the PLE is shown in parenthesis by each set of traces in W_{rms}. (—) represents TC_a while (—) represents TC_b. In both sets (around 25°C), the scale bar (—) represents a 1 °C change in temperature. The activation of the PLE emitter is shown as (—) where 1 = on and 0 = off.

source deployed. The streamer that forms remains tightly focussed and extends for many centimetres (~10 cm) from the PLE/cluster. Finally, evidence for local heating within the system is also presented.

Acknowledgements

The authors would like to thank the Office of Research and Graduate Studies at Utah State University for funds provided to SM through the Research Catalyst Grant program.

Notes and references

1 A. Suzuki, R. W. Hartel and S. Martini, *J. Food Sci.*, 2010, **75**, E208–E214.
2 M. Patrick, R. Blindt and J. Janssen, *Ultrsonics Sonochemistry*, 2004, **11**, 251–255.
3 K. Higaki, S. Ueno and K. Sato, *J. Am. Oil Chem. Soc.*, 2001, **78**, 513–518.
4 S. Ueno, R. . Ristic, K. Higaki and K. Sato, *J. Phys. Chem. B*, 2003, **107**, 4927–4935.
5 Y. Ye, A. Wagh and S. Martini, *J. Agric. Food Chem.*, 2011, **59**, 10712–10722.
6 F. Chen, H. Zhang, X. Sun, X. Wang and X. Xu, *J. Am. Oil Chem. Soc.*, 2013, **90**, 941–949.
7 H. Zhong, K. Allen and S. Martini, *Food Res. Int.*, 2014, **55**, 239–246.
8 Y. Ye and S. Martini, *J. Agric. Food Chem.*, 2015, **63**, 319–327.
9 S. Martini, A. H. Suzuki and R. W. Hartel, *J. Am. Oil Chem. Soc.*, 2008, **85**, 621–628.
10 J. M. Maruyama, A. Wagh, L. A. Gioielli, R. C. da Silva and S. Martini, *Food Res. Int.*, 2016, **86**, 54–63.
11 K. S. Suslick, S. J. Doktycz and E. B. Flint, *Ultrasonics*, 1990, **28**, 280.
12 E. B. Flint and K. S. Suslick, *Science (80-.).*, 1991, **253**, 1397–1399.
13 I. Hansson, V. Kedrinskii and K. A. Morch, *J. Appl. Phys. D Appl. Phys.*, 1982, **15**, 1725–1734.
14 I. Hansson and K. A. Morch, *J. Appl. Phys.*, 1980, **51**, 4651–4658.
15 C. J. B. Vian, P. R. Birkin and T. G. Leighton, *J. Phys. Chem. Chem. C*, 2010, **114**, 16416–16425.
16 C. K. Holland and R. E. Apfel, *IEEE Trans. Ultrason. Ferroelectr. Freq. Control*, 1989, **36**, 204–208.
17 R. E. Apfel and C. K. Holland, *Ultrasound Med. Biol.*, 1991, **17**, 179–185.
18 P. R. Birkin, D. G. Offin, C. J. B. Vian, T. G. Leighton and A. O. Maksimov, *J. Acoust. Soc. Am.*, 2011, **130**, 3297–308.
19 W. E. Rowe and W.L.Nyborg, *J. Acoust. Soc. Am.*, 1966, **39**, 965–971.
20 A. Elder, *J. Acoust. Soc. Am.*, 1959, **31**, 54–64.
21 P. R. Birkin, R. O'Connor, C. Rapple and S. S. Martinez, *J. Chem. Soc. Faraday Trans.*, 1998, **94**, 3365–3371.
22 P. R. Birkin, D. G. Offin and T. G. Leighton, *Wear*, 2005, **258**, 623–628.
23 M. E. Abdelsalam and P. R. Birkin, *Phys. Chem. Chem. Phys.*, 2002, **4**, 5340–5345.
24 M. R. Hoffmann, I. Hua and R. Hoechemer, 1996, **3**, s163–s172.
25 G. J. Price, *Introduction to Sonochemistry*, The Royal Society of Chemistry, Cambridge, 1992.
26 G. J. Price and E. J. Lenz, *Ultrasonics*, 1993, **31**, 451–456.
27 A. Weissler, H. W. Cooper and S. Snyder, *J. Am. Chem. Soc.*, 1950, **72**, 1769–1775.
28 P. R. Birkin and S. Silva-Martinez, *Chem. Commun.*, 1996, **416**, 127–138.
29 H. H. Zhang and L. A. Coury, *Anal. Chem.*, 1993, **65**, 1552–1558.
30 F. Marken, R. P. Akkermans and R. G. Compton, *J. Electroanal. Chem.*, 1996, **415**, 55–63.
31 S. Martini, R. Tejeda-Pichardo, Y. Ye, S. G. Padilla, F. K. Shen and T. Doyle, *J. Am. Oil Chem. Soc.*, 2012, **89**, 1921–1928.
32 *Manuf. quoted Fig. from datasheet*.
33 G. W. C. Kaye and T. H. Laby, *Tables of Physical and Chemical Constants and some Mathematical Functions*, Longmans, Green and Co, London, 12th edn., 1959.
34 E. A. Brujan, T. Ikeda, K. Yoshinaka and Y. Matsumoto, *Ultrason. Sonochem.*, 2011, **18**, 59–64.
35 E. A. Brujan and Y. Matsumoto, *J. Nonnewton. Fluid Mech.*, 2014, **204**, 32–37.
36 G. E. Reisman, Y.-C. Wang and C. E. Brennen, *J. Fluid Mech.*, 1998, **355**, 255–283.
37 P. R. Birkin, D. G. Offin, C. J. B. Vian and T. G. Leighton, *J. Acoust. Soc. Am.*, 2011, **130**, 3379–3388.
38 V. S. Moholkar, S. P. Sable and A. B. Pandit, *AIChE J.*, 2000, **46**, 684–694.
39 D. G. Offin, P. R. Birkin and T. G. Leighton, *Phys. Chem. Chem. Phys.*, 2014, **16**, 4982–9.
40 G. S. Settles, *Schlieren and Shadowgraph Techniques*, Springer, Berlin, 2nd edn., 2006.
41 C. Alvarez-Herrera, D. Moreno-Hernández, B. Barrientos-García and J. a. Guerrero-Viramontes, *Opt. Laser Technol.*, 2009, **41**, 233–240.
42 A. Martínez-González, J. a. Guerrero-Viramontes and D. Moreno-Hernández, *Appl. Opt.*, 2012, **51**, 3519.
43 A. Martínez-González, D. Moreno-Hernández and J. a Guerrero-Viramontes, *Appl. Opt.*, 2013, **52**, 5562–5569.
44 R. Battino, T. R. Rettich and T. Tominaga, *J. Phys. Chem. Ref. Data*, 1984, **13**, 563.
45 V. S. Moholkar, M. M. C. G. Warmoeskerken, C. D. Ohl and A. Prosperetti, *AIChE J.*, 2004, **50**, 58–64.